HHS Public Access

Author manuscript

J Physiol. Author manuscript; available in PMC 2024 March 01.

Published in final edited form as:

J Physiol. 2023 March ; 601(5): 961–978. doi:10.1113/JP284085.

Lipin1 plays complementary roles in myofiber stability and regeneration in dystrophic muscles

Abdulrahman Jama[1], **Abdullah A. Alshudukhi**[1], **Steve Burke**[2], **Lixin Dong**[3], **John Karanja Kamau**[1], **Andrew Alvin Voss**[2], **Hongmei Ren**[1]

[1]Department of Biochemistry and Molecular Biology, Wright State University, Dayton, OH, USA

[2]Department of Biological Sciences, Wright State University, Dayton, OH, USA

[3]Mumetel LLC, University Technology Park at IIT, Chicago, IL, USA.

Abstract

Duchenne muscular dystrophy (DMD) is a severe muscle wasting disorder caused by dystrophin mutation, leading to the loss of sarcolemmal integrity and resulting in progressive myofiber necrosis and impaired muscle function. Our previous studies suggest that lipin1 is important for skeletal muscle regeneration and myofiber integrity. Additionally, we discovered that mRNA expression levels of lipin1 were significantly reduced in skeletal muscle of DMD patients and mdx mouse model. To understand the role of lipin1 in dystrophic muscle, we generated dystrophin/lipin1 double knockout (DKO) mice, and compared the limb muscle pathology and function of wild-type B10, muscle-specific lipin1 deficient (lipin1^{Myf5cKO}), mdx and DKO mice. We found that further knockout of lipin1 in dystrophic muscle exhibited a more severe phenotype characterized by increased necroptosis, fibrosis and exacerbated membrane damage in DKO compared to mdx mice. In $BaCl_2$-induced muscle injury, both lipin1^{Myf5cKO} and DKO showed prolonged regeneration at day 14 post-injection, suggesting that lipin1 is critical for muscle regeneration. *In situ* contractile function assays showed that lipin1 deficiency in dystrophic muscle led to reduced specific force production. Using cell culture system, we found that lipin1 deficiency led to elevated expression levels of necroptotic markers and medium creatine kinase which could be due to sarcolemmal damage. Most importantly, restoration of lipin1 inhibited the elevation of necroptotic markers in differentiated primary lipin1-deficient myoblasts. Overall, our data suggest that lipin1 plays complementary roles in myofiber stability and muscle function in dystrophic muscles, and overexpression of lipin1 may serve as a potential therapeutic strategy for dystrophic muscles.

Graphical Abstract

To whom correspondence should be addressed: Hongmei Ren, Department of Biochemistry and Molecular Biology, Wright State University, 3640 Colonel Glenn Hwy., Dayton, OH 45435-0001, USA, Tel.: (937) 775-4693, hongmei.ren@wright.edu.

Author's contributions

H. R. and A.A.V. designed the experiments; A. J., L.D., A.A., S.B., J.K.K. performed the research; D. R. M. generated muscle force data; A. J., L.D., A.A., S.B., and J.K.K. analyzed the data; H. R. and A.A.V. wrote the manuscript, and all authors read and approved the manuscript.

Competing interests

The authors declare that they have no competing interests.

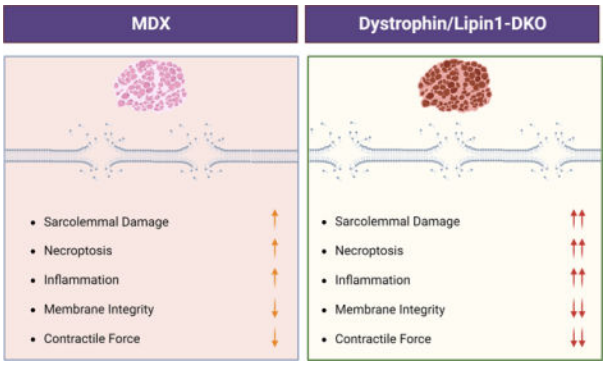

Lipin1 plays complementary roles in myofiber stability and muscle function in dystrophic muscles. Further knockout of lipin1 in dystrophic muscle exhibited increased necroptosis, inflammation, fibrosis, sarcolemma damage, and reduced force production (Figure is created with BioRender.com).

Keywords

lipin1; necroptosis; membrane integrity; skeletal muscle; muscle regeneration

Background

Duchenne muscular dystrophy (DMD) is an X-linked recessive muscle degenerative disease affecting 1 in 5000 to 1 in 6000 live male births (Mah et al. 2014; Mendell et al. 2012; Ryder et al. 2017). Patients with DMD are characterized by progressive muscle degeneration and muscle weakness leading to loss of ambulation by 8–12 years of age and premature death at 20–30 years due to respiratory and cardiac complications (Bushby et al. 2010; McDonald et al. 1995). DMD is caused by mutations in the gene that encodes dystrophin, which is the largest known gene in the human genome (Duan et al. 2021). In muscle cells, the dystrophin binds to actin filaments through its N-terminus and to the dystrophin complex through its C-terminus which is thought to provide structural stability to the plasma membrane (Norwood et al. 2000). Loss of function mutations in dystrophin triggers instability of plasma membrane during cycles of muscle contraction and relaxation that leads to muscle degeneration.

The molecular basis of skeletal muscle death has been mainly attributed to both apoptosis and necroptosis (Abdel-Salam et al. 2009; Morgan et al. 2018; Sandri et al. 1998). In particular, necroptosis has been reported to be the major contributor to myofiber death in dystrophin-deficient skeletal muscle (Morgan et al. 2018). Necroptosis is programmed necrotic cell death regulated by receptor-interacting protein kinase 1 (RIPK1), RIPK3, and mixed lineage kinase domain-like pseudokinase (MLKL) (Dhuriya et al. 2018).

In DMD, skeletal muscle degeneration is followed by ineffective muscle regeneration. Over time, the progressive impaired regeneration capability is unable to keep up with degeneration, resulting in inflammation, increased fibrotic tissue, and progressive muscle weakness and wasting. Currently there is no cure for this disease. Identifying the

molecular targets that regulate the underlying physiologic defects that predispose muscle to degeneration is critical for the treatment of DMD.

Lipin1 is a phosphatidic acid phosphatase (PAP) enzyme that catalyzes the dephosphorylation of phosphatidic acid to form diacylglycerol (Han et al. 2006; Peterfy et al. 2001). Lipin1 also acts as transcriptional coactivator of PPARs regulating their target gene expression (Finck et al. 2006). Lipin1 is mainly expressed in skeletal muscle, adipose tissue and heart (Donkor et al. 2007). Homozygous *LPIN1* gene mutations cause severe rhabdomyolysis (Michot et al. 2010). Our previous studies found that lipin1 is important for skeletal muscle regeneration (Jiang et al. 2015) and myoblast differentiation (Jama et al. 2019). Studies from ours and other groups also suggested that lipin1 is important for membrane integrity, which is indicated by Evans blue dye (EBD) leakage in lipin1 deficient skeletal muscle (Ramani Sattiraju et al. 2020; Rashid et al. 2019). Loss of membrane integrity leads to muscle degeneration that is indicated by upregulation of necroptotic markers including RIPK3 and MLKL in lipin1 deficient muscle (Ramani Sattiraju et al. 2020; Schweitzer et al. 2019). Therefore, lipin1 and dystrophin may have complementary roles in maintaining the structural and functional integrity of skeletal muscle. We predict that a combined deficiency in both lipin1 and dystrophin would lead to more severe muscle membrane damage.

To test this hypothesis, we generated lipin1 and dystrophin double deficient mice (dystrophin/lipin1 double knockout mice, DKO), and examined the role of lipin1 in the involvement of pathophysiology of muscle diseases by comparing lipin1^{Myf5cKO}, mdx, DKO and B10 WT mice. We showed that lipin1 deficiency in dystrophic muscle leads to further impaired muscle membrane integrity, upregulation of necroptotic markers, impaired myogenesis and muscle absolute force production compared to mdx mice.

Methods

Ethical Approval

All animal experiments were performed in accordance with the relevant guidelines and regulations approved by the Animal Care and Use Committee of Wright State University and approval was obtained for all experiments performed in this study (#1218). The investigators understand the ethical principles under which the journal operates and that their work complies with Journal of Physiology's animal ethics checklist. For studies performed under anesthesia, initially, mice were anesthetized with 3–5% isoflurane delivered in 100% oxygen using a rodent inhalant anesthesia apparatus (Kent Scientific Corporation). Once loss of the postural reaction and righting reflex, the mice were rapidly transferred to the nose mask, and anesthesia was maintained with 1–3% isoflurane in 100% oxygen. Anesthetic depth was assessed to assurance an adequate level of anesthesia by evaluating loss of pedal withdrawal reflex in the forelimbs and hind limbs, tail pinch reflex, and eyelid reflex. To induce skeletal muscle injury, mice were anesthetized under 1–3% isoflurane and administered a 1.2% barium chloride (BaCl2) via intramuscular injection as described in our previous study (Jiang et al. 2015). After injection, the mice were put back in a clean cage, and allowed to recover on a warm heating pad for 1h before transferring back into the animal room. Mice were checked daily for signs or symptoms of distress by the investigators

and veterinarian. Mice that display obvious changes in mobility, drinking, and eating will be euthanized. Up to date, no mice met these criteria. For tissue collection, mice were euthanized via isoflurane overdose followed by cervical dislocation prior to tissue harvest. Three–five day old pups were euthanized by narcotization with isoflurane followed by rapid decapitation with sharp scissors. All efforts were made to minimize animal suffering.

Animals

Skeletal muscle-specific lipin1 deficient (lipin1^{Myf5cKO}) mice were generated by crossing lipin1$^{fl/fl}$ with mice expressing Cre recombinase driven by Myf5 promoter as described in our previous publication(Jama et al. 2019). C57BL/10ScSnJ (B10, #000476) wild-type (WT) and mdx (#001801) mice were originally purchased from Jackson Laboratories (Bar Harbor, ME, USA). Dystrophin/lipin1-DKO mice were generated by crossing lipin1^{Myf5cKO} with mdx mice. The lipin1^{Myf5cKO} mice were on B6 background, and mdx mice on B10 background. Therefore, the DKO mice were on a mixed background. Although we used B10 as positive controls in current study, we have confirmed that there was no difference in muscle morphology, fibrosis development, inflammation markers, cell death markers, membrane integrity and force production between lipin1$^{fl/fl}$ (B6) with B10 to rule out any potential effect introduced by genetic backgrounds (data not shown). As DMD occurs primarily in males (Bushby et al. 2010), male mice at 5–7-month-old of age were used in the current study. These mice had free access to drinking water and regular chow, unless otherwise noted.

Western blotting

Muscle tissues were lysed in RIPA buffer containing 10 mM Tris-HCL (pH 7.4), 30 mM NaCl, 1 mM EDTA and 1% Nonidet P-40, supplemented with proteinase inhibitors and phosphatase inhibitors before use. Protein concentration was determined for each sample and equal amounts of proteins were used, boiled at 95°C for 5 min in 1% of SDS sample buffer and separated by 7.5–15% SDS-PAGE. Thereafter, proteins were transferred to polyvinylidene difluoride membranes (Millipore) using a Mini Trans-Blot Cell System (Bio-Rad). The membrane was blocked with 5% nonfat milk (Cell Signaling Technologies, 9999) for 1 h, and incubated with the primary antibodies in 5% BSA (Thermo Fisher Scientific, BP9704) in TBST overnight at 4°C. After probing with secondary antibodies for 1h at 25°C, protein bands were detected by using Amersham Imager 600 (GE Healthcare Life Sciences). Gapdh (Cell Signaling Technologies, 2118, 1:5000) antibody was used as a loading control. The densitometry values were normalized by the corresponding loading control densitometry values obtained from the same sample. Antibodies used include lipin1 (Cell Signaling Technology, 14906, 1:1000), RIPK1 (Cell Signaling Technology, 3493, 1:1000), RIPK3 (Cell Signaling Technology, 95702, 1:1000), MLKL (Cell Signaling Technology, 37705, 1:1000), Bax (Cell Signaling Technology, 2772, 1:1000), Bak (Cell Signaling Technology, 12105, 1:1000), CD206 (Cell Signaling Technology, 24595, 1:1000), F4/80 (Cell Signaling Technology, 70076, 1:1000), NFkB (Cell Signaling Technology, 8242, 1:1000), phospho-NFkB (Cell Signaling Technology, 3033, 1:1000), MyoD (Abcam, Ab64159, 1:1000), Mef2c (Cell Signaling Technology, 5030, 1:1000), IRS1 (Cell Signaling Technology, 2390, 1:1000), AKT (Cell Signaling Technology, 4691; 1:1000), p-AKT S473 (Cell Signaling Technology, 9271, 1:1000), p-AKT T308 (Cell Signaling Technology,

13038, 1:1000), P70S6K (Cell Signaling Technology, 2708, 1:1000), phospho-P70S6K (Cell Signaling Technology, 9205, 1:1000), along with goat anti-Rabbit IgG-HRP (Cell Signaling Technology, 7074, 1:2000).

Immunofluorescence, microscopy and image processing

The gastrocnemius muscles were frozen and sectioned at 10μm using cryostat machine. Slides were stored at −20°C. For staining, muscle sections were air dried for 1h at room temperature. The muscle sections were then hydrated with PBST, followed by blocking with 5% goat serum in PBST. To detect the colocalization of embryonic myosin heavy chain (eMyHC) with MLKL in blocking solution, sections were incubated with antibodies against eMyHC (Developmental Studies Hybridoma Bank, AB_528358, 3ug/ml) and MLKL (Abcam, ab184718, 1:200) for 1h at 37°C and subsequently with an Alexa Fluor 488- or Alexa Fluor 555-conjugated secondary antibody (Thermo Fisher Scientific, A-21411, 1:250) for 1 h in the dark at room temperature. To detect subcellular localization of eMyHC, sections were incubated with antibodies against eMyHC (Developmental Studies Hybridoma Bank, AB_528358, 3ug/ml) and laminin (Abcam, ab11575, 1:500) for 1h at 37°C before incubating with secondary antibodies. Images were obtained using an inverted microscope (Olympus, IX70) equipped with a DFC7000T camera (Leica Microsystems, Wetzlar, Germany). Indicated images were quantified by CellProfiler software.

Evans Blue Dye (EBD) Assay

Mice were injected with EBD (10 mg/ml stock in sterile saline, 0.1 ml/10 g body weight) i.p. and euthanized 24hr later. The skeletal muscles were dissected and snap-frozen in isopentane cooled optimal cutting temperature (OCT) embedding media (Tissue-Tek, Sakura-Americas). Frozen OCT blocks were cryo-sectioned at 10μm thickness and stained with laminin antibody before being analyzed by fluorescence microscopy.

$BaCl_2$-Induced Muscle Injury Model

Induction of $BaCl_2$-induced muscle injury was undertaken by injecting around 50 μl (adjusted by their body weight) of 1.2% $BaCl_2$ solution intramuscularly into the gastrocnemius muscles of adult mice (around 4 months of age) using a Hamilton syringe and 27-gauge needle. Contralateral gastrocnemius muscles injected with phosphate-buffered saline (PBS) only served as uninjured controls. Injured and uninjured muscles were then harvested at day 0 and post mortem at 6, or 14 days after injury (n = 3 mice/group) and processed for immunohistochemistry analysis.

Primary myoblasts isolation and culture conditions

Primary myoblasts were isolated from 3–5-day-old pups of lipin1^{Myf5cKO} and WT mice. Briefly, hind limb muscles were dissected and minced into pieces. Cells were dissociated enzymatically by a mixture of 2.4 U/ml dispase (Roche) and 10 mg/ml collagenase A (Roche) for 1 hour at 37 °C. The slurry was passed through a 70μm nylon mesh filter (Fisher Scientific, 22363548) and centrifuged for 5 minutes at 350g. The pellet was resuspended in 10 ml of F10 media containing 20% FBS, 100 U/ml Pen/Strep (GIBCO), and 5 ng/ml bFGF (PeproTech). Primary myoblasts were plated in collagen-coated culture plates with an F-10-

based primary myoblast growth medium (Ham's F-10 nutrient mixture containing 20% fetal calf serum and 2.5 ng/ml basic fibroblast growth factor), streptomycin, and penicillin and incubated at 37 °C supplied with 5% CO_2. Primary myoblasts were purified by pre-plating 3 times. By immunostaining with antibodies against MyoD (Thermo Fisher, MA5–12902, 2ug/ml) and Myf5 (Abcam, Ab125301, 1ug/ml), we have confirmed that the purity of isolated myoblasts was more than 97.5% (data not shown). AAV9-lipin1 was generated by the University of Pennsylvania Vector Core. AAV9-lipin1 virus infection was conducted using polybrene (10μg/ml). Differentiation of myoblasts into myotubes was initiated at ~100% confluence by cultivation in a differentiation medium (DMEM, 5% horse serum) for up to 6 days. The differentiated myotubes were then harvested for protein analysis.

Creatine Kinase (CK) Measurement

Primary myoblasts from wild-type and lipin1^{Myf5cKO} mice were plated in 6-well plates. Upon confluency, cell culture medium was replaced using differentiation medium containing high glucose DMEM supplemented with 5% horse serum to induce myogenic differentiation. Media was changed every two days. At day 6, the media from the differentiated primary cells were collected and prepared for creatine kinase activity measurement using EnzyChrom™ Creatine Kinase Assay kit (BioAssay Systems). The assay was performed in triplicate and results normalized to total protein levels using a BCA assay (Thermo Fisher).

Membrane permeability assay

Membrane permeability assay was adopted methods used in Leng et al, 2021 (Leng et al. 2021). After reaching confluence, primary myoblasts from wild-type and lipin1^{Myf5cKO} mice were differentiated for 6 days in DMEM medium supplemented with 5% horse serum. At day 6 post-differentiation, cells were washed 2 times with HBSS buffer, then incubated with 2μM of the cell impermeant form of the Ca^{2+} indicator Fluo-4 (Thermo Scientific, F14200, 2μM) for 30 minutes at 37°C. After 4 times of washing with HBSS, cellular Fluo-4 fluorescence levels were measured by fluorescence microscope (Keyence, BZ-X800LE). Background autofluorescence images taken before adding Fluo-4 were used as reference images to subtract background. Acquisition parameters were the same for all images obtained.

Contractile force measurement

In situ muscle force measurements were performed on mice anesthetized with isoflurane using a SomnoSuite low-flow anesthesia system (Kent Scientific), as described previously (Myers et al. 2021; Ramani Sattiraju et al. 2020; Wang et al. 2020). Body temperature was monitored with a SomnoSuite temperature probe and maintained at ~35℃ using a heat lamp. Force was measured from the plantar flexor muscles (lateral and medial gastrocnemius, plantaris, and soleus muscles). During the procedure to expose the muscles and sciatic nerve, the common peroneal and tibial nerves were crushed to minimize the influence of adjacent muscles. The muscles were bathed in physiological saline during surgery to prevent them from drying out. Mice were then transferred to a custom 3D-printed platform designed to eliminate movement during in situ force recordings. The mouse limb was stabilized with vertical supports and by pinning the limb into recessed areas in the platform that were filled

with Sylgard. The proximal end of the plantar flexor muscles (Achilles tendon) was attached to the lever of the force transducer (Aurora Scientific, 300D-305C dual-mode muscle lever) using 5.0 or 6.0 silk suture and a modified Miller's knot. To prevent drying, the exposed tissue was soaked in mineral oil during the contraction experiments. The full platform with the supported mouse was mounted to a micromanipulator (Thorlabs, XR25/M). To obtain optimal length, we determined the maximum twitch force while lengthening the muscle using the micromanipulator. Contractions were stimulated with platinum electrodes resting on the sciatic nerve. An S-900 Stimulator and S-910 Stimulus Isolation Unit (Dagan Corp) were used to apply 1 ms suprathreshold voltage pulses. Muscle force was recorded and digitized using pClamp10 software (Molecular Devices).

Statistical analysis

For immunostaining and Western blot, statistical analysis was performed with one-way analysis of variance (ANOVA) followed by Bonferroni's multiple comparison test to determine significant changes between groups using GraphPad Prism 9 (GraphPad Software, version 9.4.0). Data are provided as the mean ± SD number (n) of independent experiments.

Force-frequency data were fit with the following Boltzmann equation,

$$y = \frac{F_{min} - F_{max}}{1 + e\left(\frac{x - freq_{0.5}}{k}\right)} + F_{max}$$

where, x = frequency of stimulation, y = force, F_{min} = minimum force, F_{max} = maximum force, $freq_{0.5}$ = frequency giving half-max force, and k = slope factor. Data were analyzed with OriginPro 2022 (OriginLab Corp.) and reported as mean ± SD. Multiple means were compared with a one-way ANOVA, post hoc Bonferroni. For all tests, groups were considered statistically different at $\alpha = 0.05$.

Results

Lipin1 mRNA expression levels were significantly reduced in dystrophic muscle

We analyzed microarray data from Pescatori et al (Pescatori et al. 2007) available at http://www.ncbi.nlm.nih.gov/geo/ and under accession #GSE6011 to explore the decrease of lipin1 mRNA levels across different age groups of patients with DMD. Lipin1 expression levels of 19 DMD patients with age in months at biopsy are scattered along the x-axis while 14 age-matched control values are together in grey (Fig. 1A). Data were processed via robust multi-array analysis and expressed as the ratio to the mean of the control population. Overall, mRNA expression levels of lipin1 was significantly reduced by 49% during the very early phase of the disease (1.5–6 months old), suggesting that lipin1 deficiency is among the earliest cellular deficits of DMD muscles. Consistent with human data, lipin1 mRNA levels were reduced by 67% in gastrocnemius muscle from mdx mice compared to B10 WT mice (Fig. 1B), suggesting that a decrease in lipin1 mRNA expression is an early and important contributor to skeletal muscle dysfunction in DMD.

Muscle histopathology were more severe in DKO mice compared with mdx mice

To evaluate the role of lipin1 in dystrophic phenotype in our novel DKO mice, we compared their limb muscle pathology with age and gender-matched wild-type B10, muscle-specific lipin1 deficient (lipin1^{Myf5cKO}), and mdx mice (n = 4, 5–6-months-old). Consistent with what we observed previously (Jama et al. 2019), lipin1^{Myf5cKO} mice showed increased infiltration of inflammatory markers and centrally nucleated muscle fibers compared to B10 WT mice in Hematoxylin and Eosin (H&E) analysis of gastrocnemius muscle (Fig. 2A, 2B). Both mdx and DKO gastrocnemius muscle also revealed exaggerated inflammatory infiltration and significantly higher percentages of centrally-located nuclei (59% and 55% of total muscle fibers, respectively) compared to the age-matched WT mice (Fig. 2A, 2B). However, there was no significant difference in the number of centrally-nucleated myofibers between mdx and DKO mice (Fig. 2B). We also measured the cross-sectional areas of muscle fibers in these four groups (n = 6–8 mice/group). Gastrocnemius of DKO exhibited a significantly reduced mean myofiber cross-sectional area of 1184 μm^2 compared with 1660 μm^2 in gastrocnemius of mdx mice (Fig. 2C, *p value* 0.002).

Fibrosis is a hallmark of DMD, leading to muscle wasting and impaired muscle functions(Mahdy 2019). We evaluated muscle fibrosis by Picrosirius red staining in these four groups of mice (Fig. 2D and 2E). Picrosirius red staining revealed a significantly increased deposition of fibrotic tissues in DKO gastrocnemius of 6–7-month-old male mice compared to age-matched mdx mice (24% vs. 16% of total area, *p value* <0.0001), suggesting a severe fibrotic degeneration of muscles in DKO mice.

DMD is also characterized by chronic inflammation, and leukocyte (predominantly macrophages) infiltration (Le et al. 2018; Welc et al. 2020). We immunostained the muscle cross-sections for the presence of M1 macrophage using the CD68$^+$ which is a pan-macrophage proinflammatory marker (Jensen et al. 2020) (Fig. 2F). The CD68$^+$ surface area per cross-sectional area of skeletal muscle was increased to 1.26% in lipin1^{Myf5cKO} muscle compared to WT muscle, and was further increased to 3.3% in mdx and 4.7% in DKO muscle. The level of macrophages in DKO muscle increased by 142% (*p value* <0.0001) compared to mdx, suggestive of a hyper-increased pro-inflammatory state in the DKO muscles. Overall, DKO muscles clearly exhibited more severe histological lesions than mdx muscle, including centrally-nucleated fiber, fibrosis and inflammatory infiltration.

Muscle membrane integrity was more compromised in DKO compared to mdx mice

Our recent publication suggested that lipin1 deficiency alone led to a compromise in muscle membrane integrity and function in skeletal muscle-specific lipin1 deficient lipin1^{Myf5cKO} mice (Ramani Sattiraju et al. 2020). EBD, a membrane-permeable marker, has been widely used to detect membrane damage of skeletal muscle fibers (Matsuda et al. 1995; Straub et al. 1997). We found that gastrocnemius muscles of lipin1^{Myf5cKO} mice had EBD-positive muscle fibers scattered throughout the muscle sections, whereas the muscle sections of mdx mice showed clusters of EBD-positive fibers. Interestingly, the DKO mice showed patterns of both scattered and clustered EBD-positive muscle fibers (Fig. 3A). The DKO mice developed more severe muscle pathology than either mdx mice or lipin1^{Myf5cKO} mice, which is reflected by a significantly higher area of EBD uptake in DKO (12.6%) compared

to mdx muscle 7.03%) (Fig. 3B, *p-value* 0.0008, n = 5 mice/group). These data show that lipin1 plays a critical and complementary role to dystrophin in maintaining membrane integrity and that loss of lipin1 leads to a worsening of disease pathology.

Further knockdown of lipin1 in dystrophic muscle leads to enhanced necroptosis, inflammation and fibrotic markers

To evaluate how lipin1 deficiency impacts dystrophic pathology, we measured the changes in the expression of proteins involved in necroptosis, apoptosis, inflammation and fibrosis by Western blotting (Fig. 4). As shown in Fig. 4, lipin1 was deficient in lipin1^{Myf5cKO} and DKO muscle. Consistent with data shown in Fig. 1, the protein expression levels of lipin1 in gastrocnemius of mdx mice were significantly reduced by 71% (*p value* <0.0001) as compared to values from B10 WT mice.

Upregulation of necroptotic markers is an indication of enhanced necroptosis. In the gastrocnemius of DKO mice, MLKL was significantly increased by 133% compared to mdx mice (Fig. 4). Interestingly, we did not observe an obvious difference in protein expression levels of apoptotic markers including Bax and Bak between DKO mice and mdx mice suggesting that further knock out of lipin1 in dystrophic muscle may not affect skeletal muscle apoptosis but worsen necroptosis which is the major contributor for the pathology of mdx mice.

DMD is characterized by chronic inflammation and fibrosis, and both of them are mediated by a pro-fibrotic macrophage population. The NF-κB transcription factor is the master regulator of the inflammatory response. We observed increased phosphorylated NF-kB at serine 536 residues (142%, *p value* 0.0096) in DKO compared to mdx, indicating increased NF-kB activation in DKO muscle. Interestingly, the expression level of CD206, an M2 or anti-inflammatory macrophage marker, was elevated by 130% (*p value* 0.0317) in DKO muscles compared to mdx muscles, signifying a greater response from M2 macrophages to prevent deleterious inflammation. Taken together, these results indicate that there was elevated necroptosis, inflammation and fibrosis in DKO mice compared to mdx mice, which could be due to increased membrane damage.

Lipin1 deficiency in dystrophic muscle resulted in prolonged muscle regeneration in DKO mice

We evaluated the co-expression of MyHC-embryonic (eMyHC), an early myosin isoform transiently expressed by newly formed regenerating fibers with MLKL, in 5–6-month-old gastrocnemius of mdx and DKO mice (Fig. 5A). Compared to mdx muscle, DKO muscle had a large number of eMyHC$^+$ myofibers which are small in size. Surprisingly, small-size of myofibers were highly co-localized with MLKL. As shown in Fig. 5B, the Mander's coefficients of colocalization of eMyHC$^+$ myofibers with MLKL$^+$ myofibers were increased to 0.45 in DKO muscle compared to 0.18 in mdx muscle (*p value* <0.0001). We found the expression of MLKL was not detected when newly formed eMyHC-positive myofibers became mature (Size > 200μm^2). Collectively, our data indicates that maturation of newly formed muscle fibers might require the suppression of necroptotic markers, and lipin1

deficiency may lead to elevated necroptotic markers which inhibits the maturation of newly formed muscle fibers.

In addition, we observed a large number of heterogeneous eMyHC^{+} myofibers in lipin1^{Myf5cKO}, mdx and DKO mice (Fig. 5C). Interestingly, the cross-sectional areas of small-size (<100μm^2) of eMyHC^{+} myofibers account for 58% and 60% of total eMyHC^{+} myofibers in both lipin1^{Myf5cKO} and DKO muscles, respectively, compared to 34% in mdx muscle suggesting that lipin1 is critical for the maturation of newly formed muscle fibers.

We also assessed the protein expression levels of myogenic markers and protein synthesis markers in four groups of mice including B10 WT, lipin1^{Myf5cKO}, mdx and DKO mice (Fig. 5D & 5E). We found that MyoD expression levels were reduced in DKO compared to mdx mice suggesting that lipin1 deficiency in dystrophic muscle leads to impaired myogenesis (*p value* 0.0038). In addition, protein biosynthesis makers, phosphorylated AKT (p-AKT S473) and P70S6 Kinase T389 (p-P70S6K T389) were elevated in mdx muscle which might contribute to muscle pseudohypertrophy phenotype generally observed in mdx and DMD patients. Compared to mdx muscle, these protein synthesis markers were suppressed in DKO muscle by 52% (*p value* 0.0001) and 55% (*p value* 0.006), respectively.

To further understand the physiology role of lipin1 on the maturation of eMyHC^{+} myofibers, we performed a $BaCl_2$-induced regeneration study. Barium chloride solution (1.2%, 50ul) was injected into gastrocnemius to induce muscle injury (n = 3 mice/group/time point). Gastrocnemius muscles were harvested at day 6 and 14 after local $BaCl_2$ injection. To examine the temporal changes in the histological morphologies of gastrocnemius post-$BaCl_2$-induced muscle injury, regenerating gastrocnemius muscles were immunostained with eMyHC and laminin (Fig. 5F). At day 6 post-$BaCl_2$ injection, we observed extensive eMyHC-positive myofibers indicating muscle regeneration in four groups of mice at the vicinity of the injection area. By day 14 after the injection, regenerating wild-type fibers were mature and relatively homogeneous in size indicating a complete regeneration in B10 WT mice. Similarly, although regenerating muscle fibers are heterogeneous in size, eMyHC^{+} myofibers in mdx mice had been replaced by adult myosin heavy chain (Schiaffino et al. 2015) and were not visible at day 14. In contrast, DKO and lipin1^{Myf5cKO} muscle still contained a large number of eMyHC^{+} myofibers at day 14 post-injury, suggesting a prolong or abnormality in differentiation programs.

Lipin1 deficiency in dystrophic muscle led to reduced specific force production compared to mdx mice

As shown in Fig. 6, we assessed muscle function from B10 control mice (*n* = 6), mdx (*n* = 5), and DKO (*n* = 6) mice. *In situ* isometric force generation of the plantar flexor (medial and lateral gastrocnemius, plantaris, and soleus) muscles was measured in response to sciatic nerve stimulation. For reference, we included force measurements from lipin1$^{fl/fl}$ control mice (*n* = 13) and lipin1^{Myf5cKO} mice (*n* = 7), which have been published previously (Ramani Sattiraju et al. 2020). Two control lines (B10 and lipin1$^{fl/fl}$ (B6)) were used to rule out the effect of genetic backgrounds on force production. Two of the mdx mice were exposed to EBD before measuring muscle force, thereby directly linking the force measurements to our assessment of membrane damage.

The average muscle force in response to a single action potential (twitch) and during a maximal fused tetanic contraction (100 Hz stimulation) for lipin1$^{fl/fl}$, lipin1^{Myf5cKO}, mdx, and DKO are shown in Fig. 6A. To assess the response of the muscles to a full range of physiologically relevant stimulation frequencies, we measured muscle force in response to 10 or 15 action potentials stimulated from 0.3 to 100 Hz (Fig. 6B). The force-frequency relationship is shown for the absolute force (Fig. 6B top panel) and the force normalized to muscle mass (specific force, Fig. 6B bottom panel), each fitted with a Boltzmann function. As expected, there was no apparent difference in the force-frequency relationship between lipin1$^{fl/fl}$ and B10 for absolute or specific force, indicating that data from transgenic mice could be compared to either lipin1$^{fl/fl}$ or B10 mice.

It was important to consider absolute and specific force in this study because of significant differences in muscle mass between the genotypes (Fig. 6C). Relative to lipin1$^{fl/fl}$ muscle (205 ± 31.0 mg), there was significant atrophy in the lipin1^{Myf5cKO} (133 ± 24.7 mg, *p-value* 1.57×10^{-4}) and DKO (158 ± 28.2 mg, *p-value* 0.016) muscle, whereas muscle from mdx mice was hypertrophied (263 ± 29.1 mg, *p-value* 1.31×10^{-3}). A complete summary of the One-way ANOVA post hoc Bonferroni comparison for the force measurements are shown in Table 1, comparisons were made between the transgenic and lipin1$^{fl/fl}$ mouse data since we had more data from the lipin1$^{fl/fl}$ than the B10 mice. The muscle mass data indicates the mechanisms causing pseudohypertrophy in the mdx muscle (Duddy et al. 2015; Pearce et al. 1966) are not active in the lipin1^{Myf5cKO} muscle. Furthermore, the absence of lipin1 appears to eliminate pseudohypertrophy in dystrophic muscle since the DKO muscle had reduced muscle weight. Fitting the force-frequency curves with a Boltzmann fit provided an estimate of the frequency of half-maximum stimulation ($f_{1/2}$). There was no significant difference in the $f_{1/2}$ of lipin1$^{fl/fl}$ (40.7 ± 6.6 Hz) muscle compared to lipin1^{Myf5cKO} (31.5 ± 6.2 Hz, *p-value* 0.126), mdx (34.2 ± 12.3 Hz, *p-value* 0.775), or DKO (34.5 ± 5.1 Hz, *p-value* 0.745) muscle (Fig. 6C and Table 1).

In general, the average peak absolute and specific force of the lipin1^{Myf5cKO}, mdx, and DKO was reduced compared to lipin1$^{fl/fl}$ or B10 muscle throughout the force-frequency relationship (Fig. 6B). To assess this quantitatively, we compared the average responses to a single stimuli (twitch) and to maximum tetanic stimulation (100 Hz) for absolute and specific force (Fig. 6D and Table 1). Compared to lipin1$^{fl/fl}$ muscle, there was a significant decrease in absolute twitch force (Fig. 6D upper left panel) of lipin1^{Myf5cKO} and DKO muscle (Table 2). The absolute twitch force of the mdx muscle was only trending lower the lipin1$^{fl/fl}$ (*p-value* 0.083, Table 2). A similar trend was observed for the maximum absolute tetanic force (Fig. 6D, upper right panel), except that the mdx muscle also had a significantly reduced force production at 100 Hz stimulation. The specific twitch and 100 Hz force (Fig. 6D, bottom left and right panels) of the lipin1^{Myf5cKO}, mdx, and DKO were all significantly lower than lipin1$^{fl/fl}$ muscle (Table 2). The lower specific force of the mdx muscle was driven in large part, but not completely, by pseudohypertrophy. In contrast, the DKO muscle exhibited a clear reduction in absolute and specific force in response to a single stimulate or 100 Hz stimulation. The significant reductions in muscle mass and specific force indicate that the atrophied DKO muscle has substantial functional deficits.

Restoration of lipin1 suppressed necroptosis in cell culture system

To elucidate the role of lipin1 in mechanisms underlying necroptosis suppression in skeletal muscle cells, we used lipin1-CRISPR knockout C2C12 cell lines generated in our laboratory (Alshudukhi et al. 2018) and evaluated the role of lipin1 in regulating necroptotic and myogenesis markers. We found that knockdown of lipin1 in differentiated C2C12 myoblasts led to elevated protein expression levels of RIPK1, RIPK3, and MLKL by 287% (*p value* 0.009), 227% (*p value* 0.0038) and 417% (*p value* 0.0008), respectively (Fig. 7A, 7B). In contrast, lipin1 deficiency resulted in reduced expression levels of myogenesis marker MyoD by 78% (*p value* 0.02). In addition, primary myoblasts isolated from lipin1^{Myf5cKO} mice were transduced with AAV9-lipin1 to induce lipin1 expression or with AAV9-GFP followed by myoblast differentiation for 6 days. Primary myoblasts from WT mice transduced with AAV9-GFP were used as positive controls. Consistent with what we observed in C2C12 cells, primary myoblasts isolated from lipin1^{Myf5cKO} mice exhibited increased RIPK1, RIPK3 and MLKL by 334% (*p value* 0.0019), 1200% (*p value* 0.0004), and 243% (*p value* 0.0074), respectively, compared to differentiated WT myoblast controls (Fig. 7C, 7D). In contrast, restoration of AAV9-lipin1 WT virus in differentiated lipin1^{Myf5cKO} primary myoblasts suppressed elevated RIPK1, RIPK3 and MLKL by 44% (*p value* 0.0174), 46% (*p value* 0.0132) and 42% (*p value* 0.0332), respectively, and improved MyoD by 167% (*p value* 0.0351) expression, suggesting that lipin1 deficiency led to upregulation of necroptosis and downregulation of myogenesis, whereas restoring lipin1 expression ameliorated muscular degenerative phenotype by suppressing necroptosis and improving myoblast differentiation.

To further identify whether lipin1 inhibits necroptosis was due to stabilizing membrane integrity, we also measured CK levels in the cell culture medium (day 4) of differentiated primary myoblasts isolated from lipin1^{Myf5cKO} mice and WT controls (Fig. 7E). We found that lipin1 deficiency led to increased CK levels by 1.88-fold (*p value* 0.0034) in the medium suggesting that lipin1 deficiency led to increased plasma membrane permeability, which may trigger enhanced necroptosis in muscle cells.

In addition, the *in vitro* role of lipin1 in membrane integrity was assessed by using differentiated primary myoblasts isolated from WT, lipin1^{Myf5cKO} and mdx mice. Mdx myotubes were used as positive controls (Fig. 7F). At day 6 post-differentiation, cells were washed 2 times with HBSS buffer, then incubated with 2μM of cell impermeant form of the Ca^{2+} indicator Fluo-4 for 30 minutes. After washing out of the extracellular Fluo-4 with HBSS, the intracellular Fluo-4 fluorescence was measured as an indication of increased membrane permeability caused by membrane damage. The basis of this test is that more Fluo-4 will cross a plasma membrane that is damaged. We found that lipin1-deficient myoblasts had increased membrane permeability compared to WT controls suggesting that lipin1 is important for maintaining membrane integrity and lipin1 deficiency leads to leaky sarcolemma.

Discussion

Duchenne muscular dystrophy is characterized by compromised membrane integrity, severe degeneration of myofibers, loss of skeletal muscle mass, progressive muscle weakness and

significant functional impairments. In this study, we compared these hallmark symptoms in age-matched limb muscles of muscle-specific lipin1 deficient lipin1^{Myf5cKO} mice, mdx and DKO mice to evaluate the role of lipin1 in dystrophic muscles. Our data reveal that lipin1 performs different and complementary roles to dystrophin, and loss of lipin1 results in a more severe phenotype in dystrophic skeletal muscles.

Firstly, our previous study showed that loss of lipin1 alone contributes to compromised membrane integrity in lipin1 deficient muscles(Ramani Sattiraju et al. 2020). In this study, our data shows that DKO mice had even more severe membrane damage compared to mdx mice suggesting that lipin1 has overlapping roles in maintaining the structural and functional integrity of skeletal muscle as dystrophin. We further noticed that gastrocnemius muscles of lipin1^{Myf5cKO} mice had EBD-positive muscle fibers scattered throughout the muscle sections, whereas the muscle sections of mdx mice showed clusters of EBD-positive fibers. Interestingly, the DKO mice showed both patterns of scattered and clusters of EBD-positive muscle fibers. In addition, we confirmed that lipin1 deficiency in differentiated myoblasts led to increased CK release in the medium which is an indication of membrane damage, and led to elevated Fluo-4 fluorescence as an indication of leaky sarcolemma. These findings collectively suggest that lipin1 plays an important and distinct role in the protection of membrane integrity in dystrophic muscles. Future studies are warranted to identify how lipin1 regulates membrane integrity and whether lipin1 may have any role in membrane repair.

Secondly, we previously reported that loss of membrane integrity is strongly associated with necroptosis and apoptosis in the lipin1 deficient muscle (Ramani Sattiraju et al. 2020). In the present study, we found that further knock out of lipin1 in dystrophic muscle leads to the upregulation of necroptosis indicated by increased protein expression of necroptotic marker MLKL. This is confirmed in two different cell culture systems including CRISP lipin1-deficient C2C12 cells and primary myoblasts isolated from lipin1^{Myf5cKO} mice. In both cell culture systems, knockdown of lipin1 leads to significantly upregulated necroptotic markers including RIPK1, RIPK3, and MLKL, which is consistent with what we observed in skeletal muscle tissue samples.

In DMD, damage to the plasma membrane of myofibers triggers a cascade of deleterious events, cell death, inflammation, eventually fibrosis and impaired muscle function. In this study, we found enhanced macrophage infiltration indicated by CD68^{+} immunostaining and Western blotting for activation of NFkB, F4/80 and CD206. Excessive deposition of collagen and extracellular matrix elements progressively remodels and destroy normal skeletal muscle architecture in mdx mice (Mahdy 2019; Mann et al. 2011). Using Picro Sirius red staining, we also found that further knock out of lipin1 in dystrophic muscle leads to enhanced fibrosis. Our data suggest that loss of lipin1 other than the absence of dystrophin also contributes to the degeneration of skeletal muscle fibers in dystrophic muscles.

Thirdly, in this study, we also found that lipin1 is important for skeletal muscle regeneration which is consistent with our previous findings(Jama et al. 2019; Jiang et al. 2015). Compared to dystrophic muscle, further knockout of lipin1 led to increased small-size

of eMyHC$^+$ muscle fibers (<100μm^2), highly colocalized with MLKL, suggesting that lipin1 deficiency may lead to elevation of cell death which inhibits the maturation of eMyHC$^+$ myofibers. The role of lipin1 on the maturation of eMyHC$^+$ myofibers was further confirmed in our $BaCl_2$-induced regeneration study. Lipin1 deficiency in dystrophic muscle resulted in a prolonged or abnormality in muscle regeneration at day 14 after $BaCl_2$ injury. eMyHC$^+$ has also been reported to be activated by the myogenic regulatory factors MyoD through binding to the E-box elements in the proximal promoter region (Beylkin et al. 2006; Konig et al. 2002; Schiaffino et al. 2015). Our Western blot analysis suggests that lipin1 deficiency leads to reduced expression levels of MyoD in DKO mice which could result in the inhibition of eMyHC maturation. In addition, lipin1 has been reported to be required during the myoblast fusion process in our previous study (Jiang et al. 2015), which could also contribute to small-size of eMyHC$^+$ muscle fibers formation. Incomplete fusion of regenerating myotubes may lead to forked fibers, muscle weakness, and wasting (Ciciliot et al. 2010). It is widely accepted that repetitive cycles of muscle degeneration and regeneration leads to an exhaustion of regenerative capacity in advanced dystrophic muscles (Flanigan 2014).

Several other proteins have been reported to play an important role in strengthening muscle membrane integrity including utrophin, α7 integrin, sarcospan, laminin, biglycan, PGC1α&β, nNOS, GalNAC and Adam12 in the absence of dystrophin leading to histological and functional improvement in dystrophic mice (Amenta et al. 2011; Burkin et al. 2001; Chan et al. 2014; Gibbs et al. 2016; Goudenege et al. 2010; Moghadaszadeh et al. 2003; Nguyen et al. 2002; Tidball et al. 2004; Tinsley et al. 1996). Since mini-dystrophin or microdystrophin may not provide full functional improvement, combinations of dystrophin with these proteins may result in additive functional benefits than either single approach alone. Therefore, identifying the proteins which can stabilize membrane integrity in dystrophic muscle will contribute to the development of potential combination therapies for DMD patients, especially for older patients. Our data suggest that increasing the expression level of lipin1 may enhance muscle regeneration and present promising as a complementary therapy for older DMD patients. In particular, overexpression of lipin1 using AAV9-lipin1 mitigated the expression of necroptotic markers in differentiated primary myoblasts. It is likely that lipin1 restoration strengthened membrane integrity, in turn suppressed necroptosis.

Moreover, we found that the protein expression levels of lipin1 expression are substantially reduced both in DMD patients and mdx muscle. However, our data indicate that lipin1 has distinct and complementary roles in regulating muscle membrane integrity, loss of lipin1 leads to a worsening of disease pathology. Therefore, lipin1 could be a potential therapeutic target and restoring the expression of lipin1 to a physiological level may serve as an effective complementary treatment in dystrophic muscles.

In future studies, we will evaluate whether overexpression of lipin1 could strengthen membrane integrity acting as a novel regulator to counteract dystrophic pathologies. We will determine the mechanism of lipin1 downregulation in dystrophic muscle. Interestingly, a previous study showed that the knockdown of dystrophin in myotubes from B10 mice using RNAi significantly reduced lipin1 expression (Ghahramani Seno et al. 2010). We will

utilize the same *in vitro* assay system to knock down dystrophin or lipin1 in myotubes to determine how dystrophin influences lipin1 expression.

In conclusion, our study has demonstrated that lipin1 expression is dramatically reduced in dystrophic muscles. Loss of lipin1 contributes to compromised membrane integrity, elevated skeletal muscle degeneration and impaired muscle regeneration, which may underlie phenotypes of progressive weakness and loss of muscle mass in dystrophic muscles. In addition, our data also suggest that lipin1 could serve as a potential therapeutic target for the treatment of patients with DMD.

Supplementary Material

Refer to Web version on PubMed Central for supplementary material.

Funding

This project was supported by an NIH grant (5R01AR077574) and DoD Idea Development Award awarded to H.R., and an NIH/NINDS R15NS099850 to A.A.V. The authors declare no conflicts of interest.

Biography

Abdulrahman Jama received his B.S. in Molecular genetics from Ohio State University and M.S. in Biochemistry & Molecular Biology from Wright State University. Currently he is a PhD student in the Department of Biochemistry & Molecular Biology at Wright State University. His overall research goal is to understand the role of lipin1 in the pathophysiology of Duchenne muscular dystrophy.

Data availability statement

All data is available from the corresponding author upon reasonable request from a qualified researcher.

List of abbreviations

EBD	Evans blue dye
PA	phosphatidic acid
PAP	phosphatidic acid phosphatase
DAG	diacylglycerol
WT	wild-type
eMyHC	embryonic myosin heavy chain

RIPK	receptor-interacting serine/threonine-protein kinase
MLKL	mixed-lineage kinase domain-like protein
OCT	optimal cutting temperature

References

Abdel-Salam E, Abdel-Meguid I and Korraa SS. (2009). Markers of degeneration and regeneration in Duchenne muscular dystrophy. Acta Myol 28, 94–100. [PubMed: 20476668]

Alshudukhi AA, Zhu J, Huang DT, Jama A, Smith JD, Wang QJ, Esser KA and Ren HM. (2018). Lipin-1 regulates Bnip3-mediated mitophagy in glycolytic muscle. Faseb Journal 32, 6796–6807. [PubMed: 29939786]

Amenta AR, Yilmaz A, Bogdanovich S, McKechnie BA, Abedi M, Khurana TS and Fallon JR. (2011). Biglycan recruits utrophin to the sarcolemma and counters dystrophic pathology in mdx mice. Proceedings of the National Academy of Sciences of the United States of America 108, 762–767. [PubMed: 21187385]

Beylkin DH, Allen DL and Leinwand LA. (2006). MyoD, Myf5, and the calcineurin pathway activate the developmental myosin heavy chain genes. Dev Biol 294, 541–553. [PubMed: 16584724]

Burkin DJ, Wallace GQ, Nicol KJ, Kaufman DJ and Kaufman SJ. (2001). Enhanced expression of the alpha 7 beta 1 integrin reduces muscular dystrophy and restores viability in dystrophic mice. J Cell Biol 152, 1207–1218. [PubMed: 11257121]

Bushby K, Finkel R, Birnkrant DJ, Case LE, Clemens PR, Cripe L, Kaul A, Kinnett K, McDonald C, Pandya S, Poysky J, Shapiro F, Tomezsko J and Constantin C. (2010). Diagnosis and management of Duchenne muscular dystrophy, part 2: implementation of multidisciplinary care. Lancet Neurol 9, 177–189. [PubMed: 19945914]

Bushby K, Finkel R, Birnkrant DJ, Case LE, Clemens PR, Cripe L, Kaul A, Kinnett K, McDonald C, Pandya S, Poysky J, Shapiro F, Tomezsko J, Constantin C and Working DCC. (2010). Diagnosis and management of Duchenne muscular dystrophy, part 1: diagnosis, and pharmacological and psychosocial management. Lancet Neurology 9, 77–93. [PubMed: 19945913]

Chan MC, Rowe GC, Raghuram S, Patten IS, Farrell C and Arany Z. (2014). Post-natal induction of PGC-1 alpha protects against severe muscle dystrophy independently of utrophin. Skeletal Muscle 4

Ciciliot S and Schiaffino S. (2010). Regeneration of Mammalian Skeletal Muscle: Basic Mechanisms and Clinical Implications. Current Pharmaceutical Design 16, 906–914. [PubMed: 20041823]

Dhuriya YK and Sharma D. (2018). Necroptosis: a regulated inflammatory mode of cell death. Journal of Neuroinflammation 15

Donkor J, Sariahmetoglu M, Dewald J, Brindley DN and Reue K. (2007). Three mammalian lipins act as phosphatidate phosphatases with distinct tissue expression patterns. Journal of Biological Chemistry 282, 3450–3457. [PubMed: 17158099]

Duan DS, Goemans N, Takeda S, Mercuri E and Aartsma-Rus A. (2021). Duchenne muscular dystrophy. Nature Reviews Disease Primers **77**

Duddy W, Duguez S, Johnston H, Cohen TV, Phadke A, Gordish-Dressman H, Nagaraju K, Gnocchi V, Low S and Partridge T. (2015). Muscular dystrophy in the mdx mouse is a severe myopathy compounded by hypotrophy, hypertrophy and hyperplasia. Skeletal Muscle 5

Finck BN, Gropler MC, Chen ZJ, Leone TC, Croce MA, Harris TE, Lawrence JC and Kelly DP. (2006). Lipin 1 is an inducible amplifier of the hepatic PGC-1 alpha/PPAR alpha regulatory pathway. Cell Metabolism 4, 199–210. [PubMed: 16950137]

Flanigan KM (2014). Duchenne and Becker muscular dystrophies. Neurol Clin 32, 671–688, viii. [PubMed: 25037084]

Ghahramani Seno MM, Trollet C, Athanasopoulos T, Graham IR, Hu P and Dickson G. (2010). Transcriptomic analysis of dystrophin RNAi knockdown reveals a central role for dystrophin in muscle differentiation and contractile apparatus organization. BMC Genomics 11, 345. [PubMed: 20515474]

Gibbs EM, Marshall JL, Ma E, Nguyen TM, Hong G, Lam JS, Spencer MJ and Crosbie-Watson RH. (2016). High levels of sarcospan are well tolerated and act as a sarcolemmal stabilizer to address skeletal muscle and pulmonary dysfunction in DMD. Human Molecular Genetics 25, 5395–5406. [PubMed: 27798107]

Goudenege S, Lamarre Y, Dumont N, Rousseau J, Frenette J, Skuk D and Tremblay JP. (2010). Laminin-111: a potential therapeutic agent for Duchenne muscular dystrophy. Mol Ther 18, 2155–2163. [PubMed: 20683444]

Han GS, Wu WI and Carman GM. (2006). The Saccharomyces cerevisiae lipin homolog is a Mg2+-dependent phosphatidate phosphatase enzyme. Journal of Biological Chemistry 281, 9210–9218. [PubMed: 16467296]

Jama A, Huang DT, Alshudukhi AA, Chrast R and Ren HM. (2019). Lipin1 is required for skeletal muscle development by regulating MEF2c and MyoD expression. Journal of Physiology-London 597, 889–901.

Jensen SM, Bechshoft CJL, Heisterberg MF, Schjerling P, Andersen JL, Kjaer M and Mackey AL. (2020). Macrophage Subpopulations and the Acute Inflammatory Response of Elderly Human Skeletal Muscle to Physiological Resistance Exercise. Front Physiol 11, 811. [PubMed: 32792975]

Jiang WH, Zhu J, Zhuang X, Zhang XP, Luo T, Esser KA and Ren HM. (2015). Lipin1 Regulates Skeletal Muscle Differentiation through Extracellular Signal-regulated Kinase (ERK) Activation and Cyclin D Complex-regulated Cell Cycle Withdrawal. Journal of Biological Chemistry 290, 23646–23655. [PubMed: 26296887]

Konig S, Burkman J, Fitzgerald J, Mitchell M, Su L and Stedman H. (2002). Modular organization of phylogenetically conserved domains controlling developmental regulation of the human skeletal myosin heavy chain gene family. J Biol Chem 277, 27593–27605. [PubMed: 11971910]

Le G, Novotny SA, Mader TL, Greising SM, Chan SSK, Kyba M, Lowe DA and Warren GL. (2018). A moderate oestradiol level enhances neutrophil number and activity in muscle after traumatic injury but strength recovery is accelerated. Journal of Physiology-London 596, 4665–4680.

Leng L, Dong X, Gao X, Ran N, Geng M, Zuo B, Wu Y, Li W, Yan H, Han G and Yin H. (2021). Exosome-mediated improvement in membrane integrity and muscle function in dystrophic mice. Mol Ther 29, 1459–1470. [PubMed: 33333294]

Mah JK, Korngut L, Dykeman J, Day L, Pringsheim T and Jette N. (2014). A systematic review and meta-analysis on the epidemiology of Duchenne and Becker muscular dystrophy. Neuromuscul Disord 24, 482–491. [PubMed: 24780148]

Mahdy MAA (2019). Skeletal muscle fibrosis: an overview. Cell and Tissue Research 375, 575–588. [PubMed: 30421315]

Mann CJ, Perdiguero E, Kharraz Y, Aguilar S, Pessina P, Serrano AL and Munoz-Canoves P. (2011). Aberrant repair and fibrosis development in skeletal muscle. Skelet Muscle 1, 21. [PubMed: 21798099]

Matsuda R, Nishikawa A and Tanaka H. (1995). Visualization of Dystrophic Muscle-Fibers in Mdx Mouse by Vital Staining with Evans Blue - Evidence of Apoptosis in Dystrophin-Deficient Muscle. Journal of Biochemistry 118, 959–964. [PubMed: 8749313]

McDonald CM, Abresch RT, Carter GT, Fowler WM Jr., Johnson ER, Kilmer DD and Sigford BJ. (1995). Profiles of neuromuscular diseases. Duchenne muscular dystrophy. Am J Phys Med Rehabil 74, S70–92. [PubMed: 7576424]

Mendell JR, Shilling C, Leslie ND, Flanigan KM, al-Dahhak R, Gastier-Foster J, Kneile K, Dunn DM, Duval B, Aoyagi A, Hamil C, Mahmoud M, Roush K, Bird L, Rankin C, Lilly H, Street N, Chandrasekar R and Weiss RB. (2012). Evidence-based path to newborn screening for Duchenne muscular dystrophy. Ann Neurol 71, 304–313. [PubMed: 22451200]

Michot C, Hubert L, Brivet M, De Meirleir L, Valayannopoulos V, Muller-Felber W, Venkateswaran R, Ogier H, Desguerre I, Altuzarra C, Thompson E, Smitka M, Huebner A, Husson M, Horvath R, Chinnery P, Vaz FM, Munnich A, Elpeleg O, Delahodde A, ... (2010). LPIN1 gene mutations: a major cause of severe rhabdomyolysis in early childhood. Hum Mutat 31, E1564–1573. [PubMed: 20583302]

Moghadaszadeh B, Albrechtsen R, Guo LT, Zaik M, Kawaguchi N, Borup RH, Kronqvist P, Schroder HD, Davies KE, Voit T, Nielsen FC, Engvall E and Wewer UM. (2003). Compensation for

dystrophin-deficiency: ADAM12 overexpression in skeletal muscle results in increased alpha 7 integrin, utrophin and associated glycoproteins. Hum Mol Genet 12, 2467–2479. [PubMed: 12915458]

Morgan JE, Prola A, Mariot V, Pini V, Meng J, Hourde C, Dumonceaux J, Conti F, Relaix F, Authier FJ, Tiret L, Muntoni F and Bencze M. (2018). Necroptosis mediates myofibre death in dystrophin-deficient mice. Nat Commun 9, 3655. [PubMed: 30194302]

Myers JH, Denman K, DuPont C, Hawash AA, Novak KR, Koesters A, Grabner M, Dayal A, Voss AA and Rich MM. (2021). The mechanism underlying transient weakness in myotonia congenita. Elife 10

Nguyen HH, Jayasinha V, Xia B, Hoyte K and Martin PT. (2002). Overexpression of the cytotoxic T cell GalNAc transferase in skeletal muscle inhibits muscular dystrophy in mdx mice. Proc Natl Acad Sci U S A 99, 5616–5621. [PubMed: 11960016]

Norwood FL, Sutherland-Smith AJ, Keep NH and Kendrick-Jones J. (2000). The structure of the N-terminal actin-binding domain of human dystrophin and how mutations in this domain may cause Duchenne or Becker muscular dystrophy. Structure 8, 481–491. [PubMed: 10801490]

Pearce GW, Pearce JM and Walton JN. (1966). The Duchenne type muscular dystrophy: histopathological studies of the carrier state. Brain 89, 109–120. [PubMed: 5910897]

Pescatori M, Broccolini A, Minetti C, Bertini E, Bruno C, D'Amico A, Bernardini C, Mirabella M, Silvestri G, Giglio V, Modoni A, Pedemonte M, Tasca G, Galluzzi G, Mercuri E, Tonali PA and Ricci E. (2007). Gene expression profiling in the early phases of DMD: a constant molecular signature characterizes DMD muscle from early postnatal life throughout disease progression. FASEB J 21, 1210–1226. [PubMed: 17264171]

Peterfy M, Phan J, Xu P and Reue K. (2001). Lipodystrophy in the fld mouse results from mutation of a new gene encoding a nuclear protein, lipin. Nat Genet 27, 121–124. [PubMed: 11138012]

Ramani Sattiraju S, Jama A, Alshudukhi AA, Edward Townsend N, Reynold Miranda D, Reese RR, Voss AA and Ren H. (2020). Loss of membrane integrity drives myofiber death in lipin1-deficient skeletal muscle. Physiol Rep 8, e14620. [PubMed: 33113595]

Rashid T, Nemazanyy I, Paolini C, Tatsuta T, Crespin P, de Villeneuve D, Brodesser S, Benit P, Rustin P, Baraibar MA, Agbulut O, Olivier A, Protasi F, Langer T, Chrast R, de Lonlay P, de Foucauld H, Blaauw B and Pende M. (2019). Lipin1 deficiency causes sarcoplasmic reticulum stress and chaperone-responsive myopathy. EMBO J 38

Ryder S, Leadley RM, Armstrong N, Westwood M, de Kock S, Butt T, Jain M and Kleijnen J. (2017). The burden, epidemiology, costs and treatment for Duchenne muscular dystrophy: an evidence review. Orphanet J Rare Dis 12, 79. [PubMed: 28446219]

Sandri M, Minetti C, Pedemonte M and Carraro U. (1998). Apoptotic myonuclei in human Duchenne muscular dystrophy. Lab Invest 78, 1005–1016. [PubMed: 9714187]

Schiaffino S, Rossi AC, Smerdu V, Leinwand LA and Reggiani C. (2015). Developmental myosins: expression patterns and functional significance. Skelet Muscle 5, 22. [PubMed: 26180627]

Schweitzer GG, Collier SL, Chen ZJ, McCommis KS, Pittman SK, Yoshino J, Matkovich SJ, Hsu FF, Chrast R, Eaton JM, Harris TE, Weihl CC and Finck BN. (2019). Loss of lipin 1-mediated phosphatidic acid phosphohydrolase activity in muscle leads to skeletal myopathy in mice. Faseb Journal 33, 652–667. [PubMed: 30028636]

Straub V, Rafael JA, Chamberlain JS and Campbell KP. (1997). Animal models for muscular dystrophy show different patterns of sarcolemmal disruption. Journal of Cell Biology 139, 375–385. [PubMed: 9334342]

Tidball JG and Wehling-Henricks M. (2004). Expression of a NOS transgene in dystrophin-deficient muscle reduces muscle membrane damage without increasing the expression of membrane-associated cytoskeletal proteins. Molecular Genetics and Metabolism 82, 312–320. [PubMed: 15308129]

Tinsley JM, Potter AC, Phelps SR, Fisher R, Trickett JI and Davies KE. (1996). Amelioration of the dystrophic phenotype of mdx mice using a truncated utrophin transgene. Nature 384, 349–353. [PubMed: 8934518]

Wang X, Burke SRA, Talmadge RJ, Voss AA and Rich MM. (2020). Depressed neuromuscular transmission causes weakness in mice lacking BK potassium channels. J Gen Physiol 152

Welc SS, Wehling-Henricks M, Kuro-o M, Thomas KA and Tidball JG. (2020). Modulation of Klotho expression in injured muscle perturbs Wnt signalling and influences the rate of muscle growth. Experimental Physiology 105, 132–147. [PubMed: 31724771]

Key Points

We identified that lipin1 mRNA expression levels are significantly reduced in skeletal muscles of DMD patients and mdx mice.

We found that further depletion of lipin1 in skeletal muscles of mdx mice induces more severe dystrophic phenotypes including enhanced myofiber sarcolemma damage, muscle necroptosis, inflammation, fibrosis, and reduced specific force production.

Lipin1 deficiency leads to elevated expression levels of necroptotic markers while restoration of lipin1 inhibits their expression.

Our results suggest that lipin1 is functionally complementary to dystrophin in muscle membrane integrity and muscle regeneration.

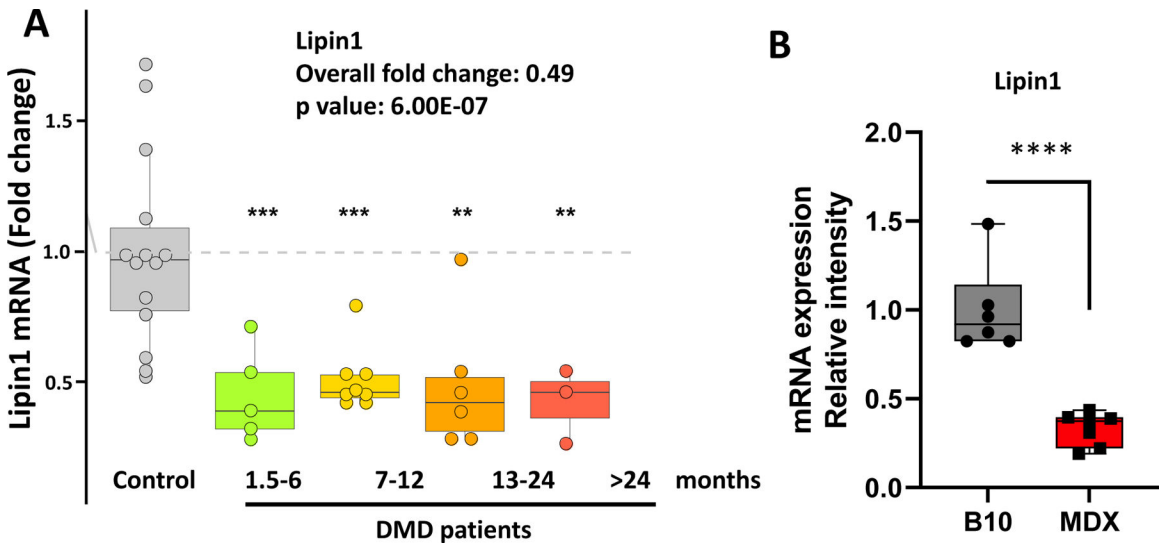

Fig. 1. Lipin1 expression levels significantly reduced in dystrophic muscles of human DMD patients and mdx mice.

(A) Changes in transcript abundance of DMD patients are expressed as a ratio to the control mean. **(B)** mRNA expression of lipin1 gene in gastrocnemius of mdx mice (n = 6–7 male mice/group, 5–6-month-old). Significance was assessed by t-test; **p < 0.01, ***p < 0.001.

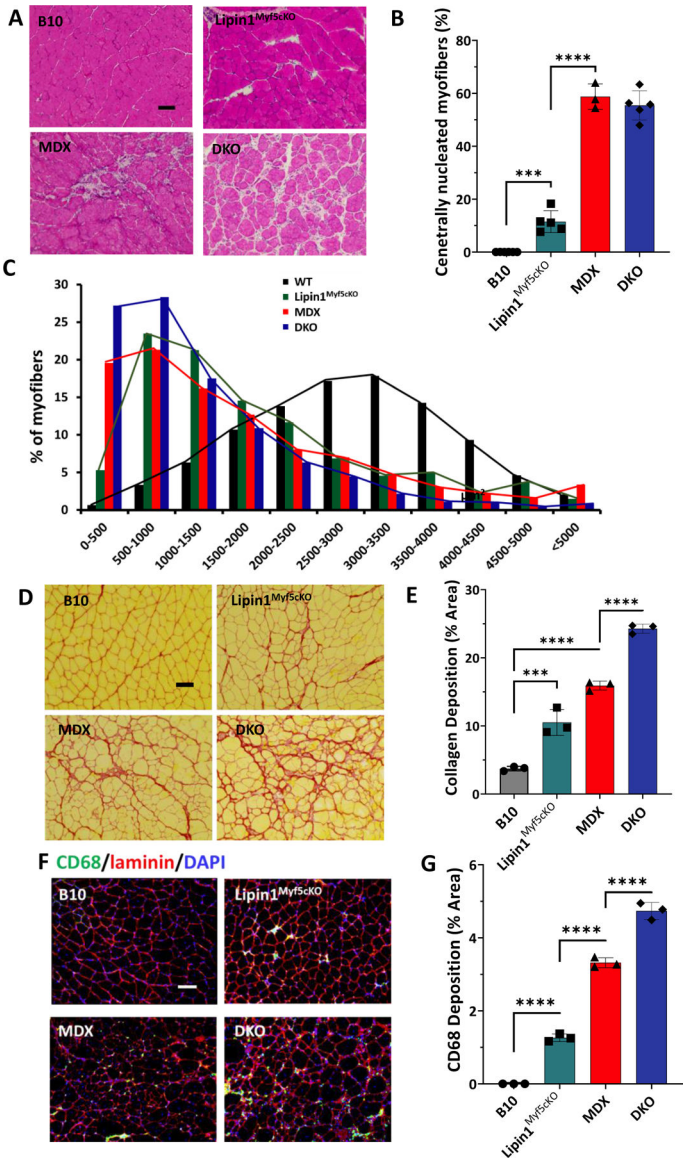

Fig. 2. Severe histopathology in gastrocnemius muscle of dystrophin/lipin1 double knock-out (DKO) mice compared to mdx and lipin1–deficient lipin1^{Myf5cKO} mice.

(A) H&E stained sections**, (B)** Quantification of centrally nucleated fibers per total fiber numbers**, (C)** cross-sectional areas, **(D)** Picrosirius red staining, **(E)** quantification of collagen area normalized to the total muscle area (mm^2), **(F)** CD68 staining and **(G)** quantification analysis of CD68+ area normalized to the total muscle area. N = 3–5 male mice/group. Scale bars = 100 μm. ***p < 0.005.

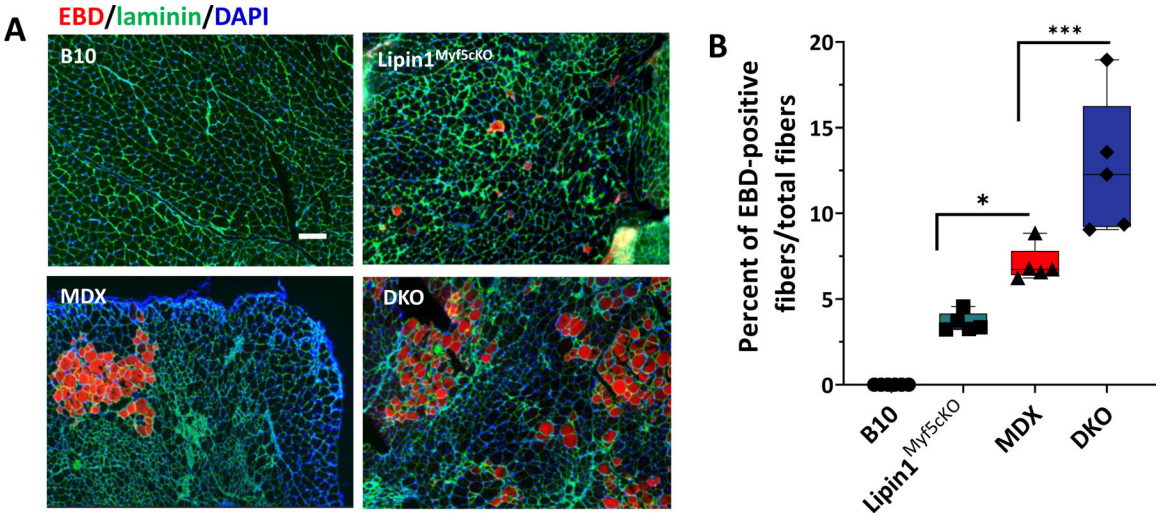

Fig. 3. Lipin1 plays a critical and complementary role to dystrophin in maintaining membrane integrity.

(A) EBD uptake of gastrocnemius muscle sections from lipin1^{Myf5cKO}, mdx, and DKO mice. Scar bar = 200μm. **(B)** Quantification analysis of EBD-positive muscle fiber expressed as the percentage of the total number of muscle fibers in each mouse. N = 4–6 mice/group. *p<0.05.

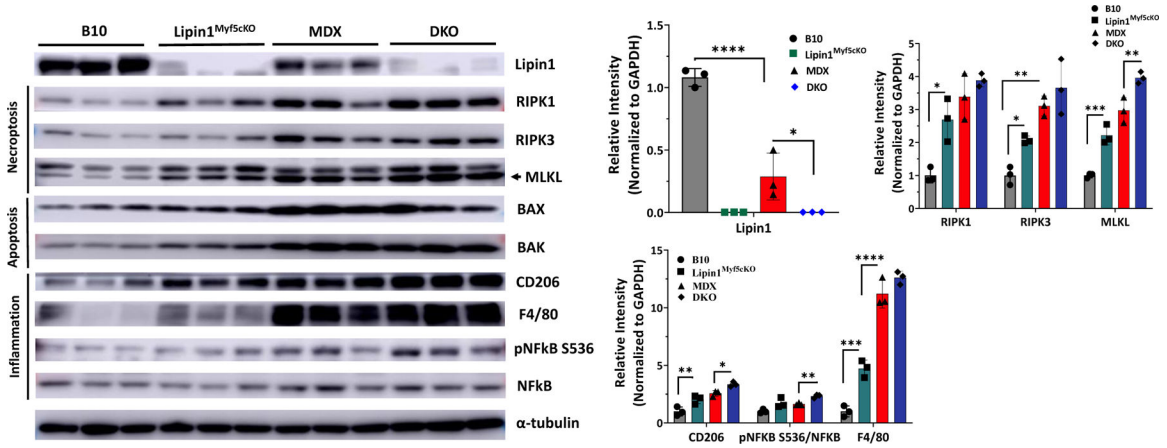

Fig. 4. Further knockdown of lipin1 in dystrophic muscle leads to elevated expression levels of necroptotic, apoptotic, and inflammation markers.

(A) Representative immunoblots and **(B)** quantitative analysis of necroptotic (RIPK1, RIPK3, and MLKL), apoptotic (BAX and BAK), and inflammation (F4/80, CD206 and NF-KB) markers in indicated mice. N = 3 mice/group. *p < 0.05; **p < 0.01, ***p < 0.005.

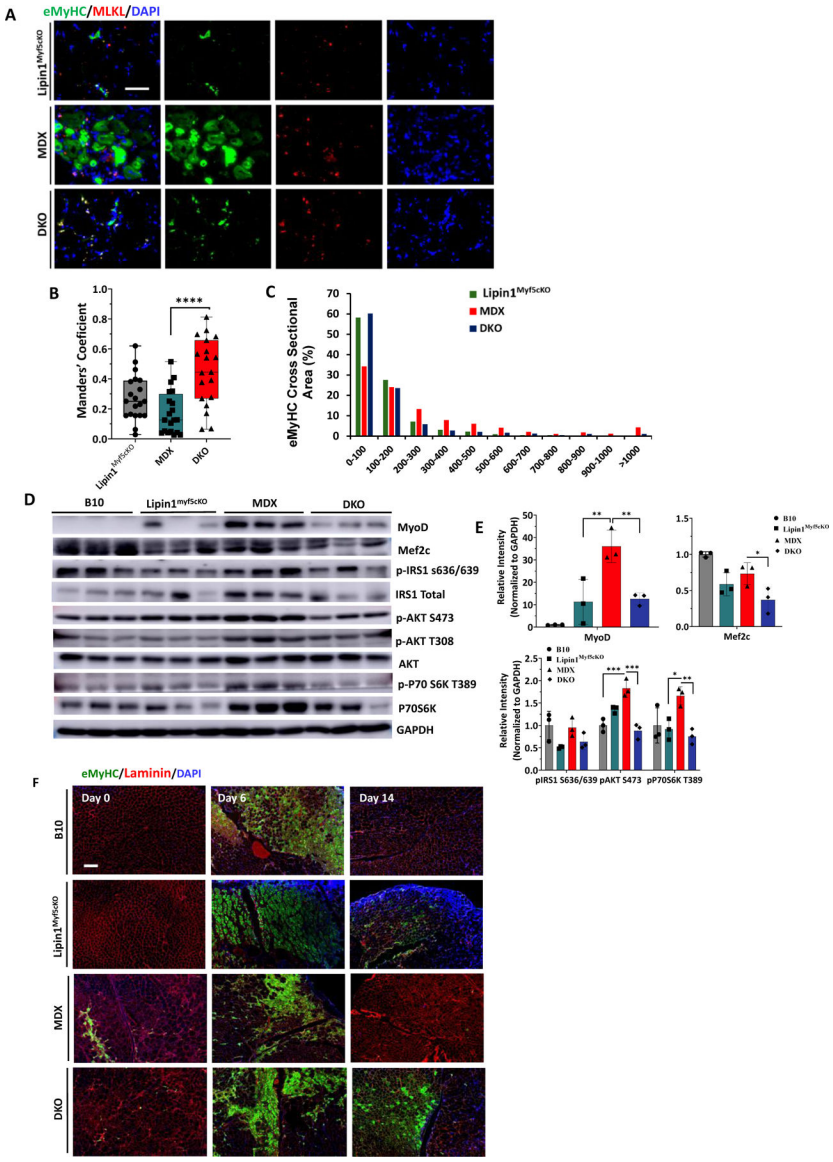

Fig. 5. Lipin1 deficiency impairs myogenesis in dystrophic muscles.

(A) Colocalization of eMyHC (green) with MLKL (red), and **(B)** Manders' correlation coefficient analysis as a measure of colocalization of eMyHC^{+} with MLKL^{+} muscle fibers in gastrocnemius of lipin1^{Myf5cKO} (turquoise), mdx (red), and DKO (blue) mice (n = 3 mice/group). (1 = highest colocalization and 0 = zero colocalization) **(C)** Histogram showing the percentage of eMyHC muscle fiber size distributions in 5–7-month-old B10 (WT), lipin1^{Myf5cKO}, mdx, and DKO mouse measured by CellProfiler software. Western blot **(D)** and quantification **(E)** analysis of myogenesis and protein synthesis markers in gastrocnemius of B10 (grey), lipin1^{Myf5cKO} (turquoise), mdx (red), and DKO (blue) mice at 5–6-month-old of age. **(F)** Immunostaining with antibodies against eMyHC (green) and laminin (red) of uninjured TA muscles (day 0) and injured gastrocnemius muscles harvested on days 6 and 14 after injury. To induce acute skeletal muscle injury, 1.2% $BaCl_2$ solution or PBS was injected into the gastrocnemius of each mouse. Injured and uninjured muscles were

harvested at 0 days (before injury) and post mortem at 6 or 14 days after injury. Scale bars = 100 μm. N = 3 mice/group. *p<0.05.

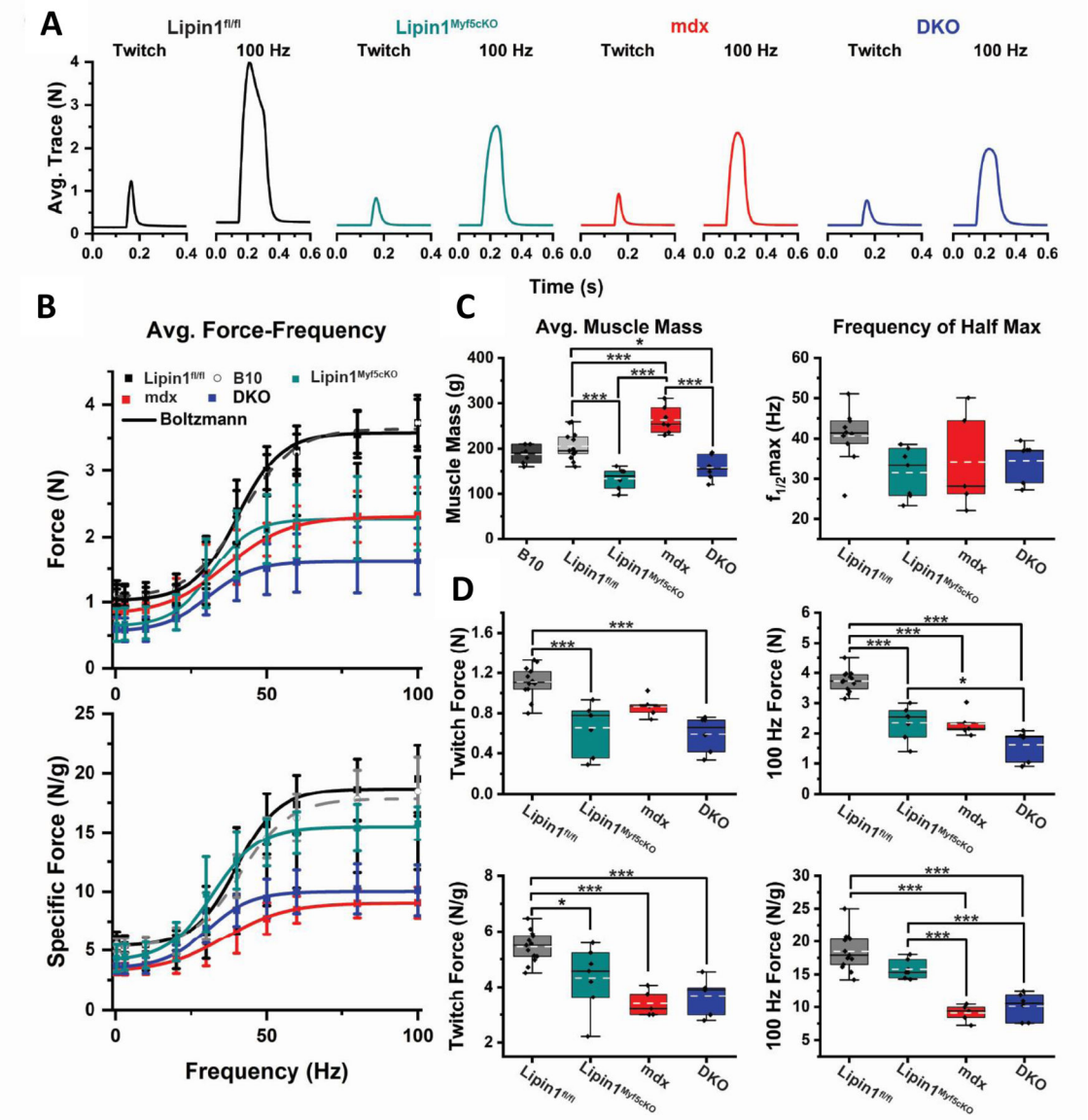

Fig. 6. Reduced specific force production in DKO mice.

(A) Average twitch and maximum tetanic (100Hz) force production in the lipin1$^{fl/fl}$ (black), lipin1^{Myf5cKO} (turquoise), mdx (red), and DKO (blue) skeletal muscle. **(B)** The force-frequency relationships of the absolute (top panel) and specific (bottom panel) force values from lipin1$^{fl/fl}$ (black), B10 (gray), lipin1^{Myf5cKO} (turquoise), mdx (red), and DKO (blue) skeletal muscle. Values are shown as mean ± SD. **(C)** Box-and-whisker plots of the muscle mass and frequency at which half the maximum force was generated ($f_{1/2}$). **(D)** Box-and-whisker plots of the peak force during twitch and 100 Hz maximum contractions, measured as absolute force (top row) and specific force (bottom row). Each box indicates the 25–75% interquartile range, the whiskers indicate 1.5 times the interquartile range, the black solid line indicates the median, the dashed white line indicates the mean, and each data point is shown as a diamond. Data in C and D were compared using a one-way ANOVA, post hoc

Bonferroni. *p < 0.05 and ***p < 0.005. Data from n = 13 lipin1$^{fl/fl}$, 6 B10, 7 lipin1^{Myf5cKO}, 5 mdx, and 6 DKO mice.

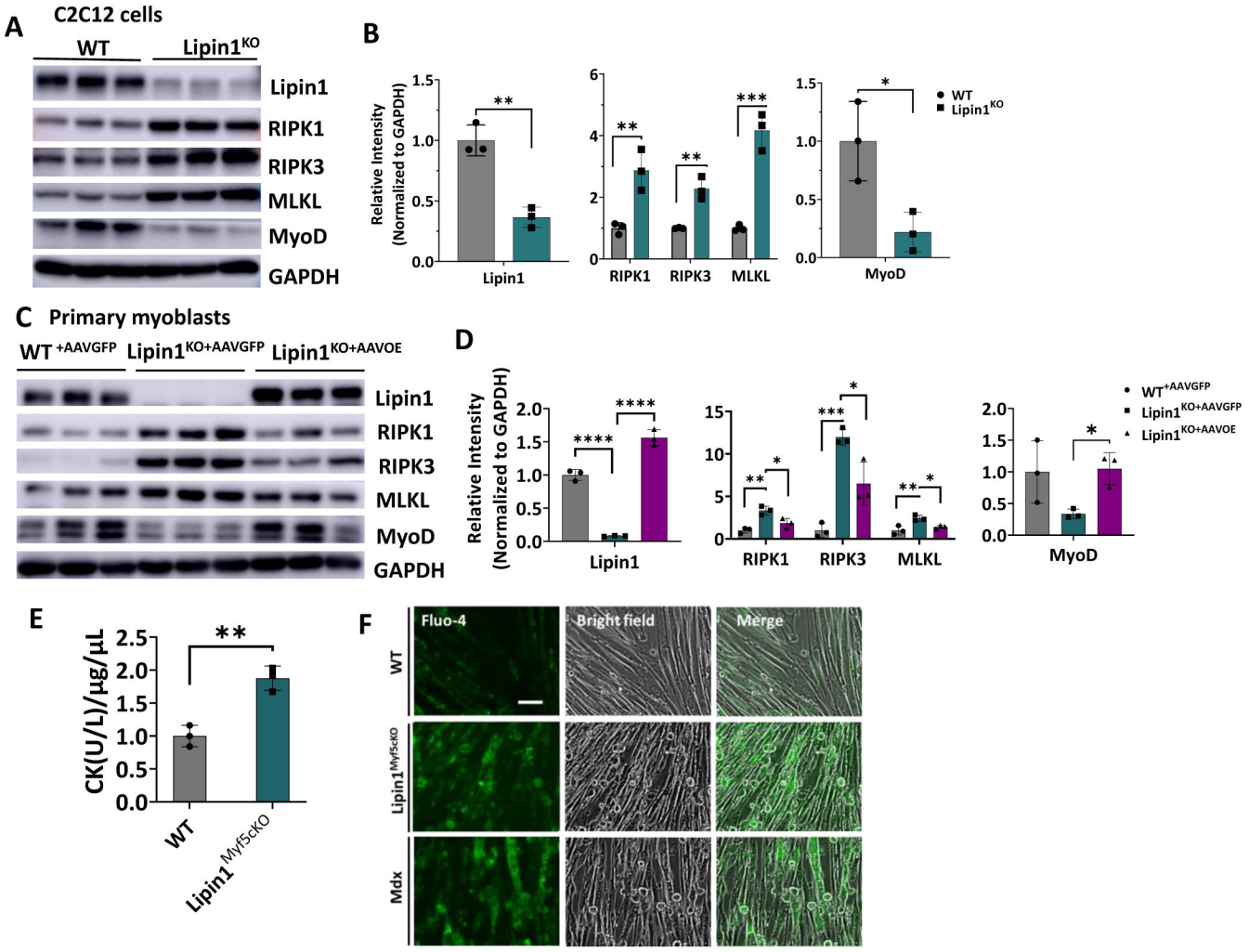

Fig. 7. *In vitro* restoration of lipin1 protein suppresses necrotic cell death in lipin1-deficient myoblasts.

(A) Protein expression levels and **(B)** quantification analysis of indicated markers analyzed in lipin1-CRISPR-knockout C2C12 myoblasts after the onset of differentiation for 6 days. **(C)** Protein expression levels and **(D)** quantification analysis of necroptotic makers and myogenesis markers measured by Western blotting after primary myoblasts isolated from WT and lipin1^{Myf5cKO} mice, which were infected with either AAV-lipin1 or AAV-GFP followed by differentiation for 6 days. **(E)** CK levels in cell culture medium of differentiated WT and lipin1-deficient primary myoblasts collected at day 4 post-differentiation treatment and normalized to total protein lysates. **(F)** Primary myoblasts from WT and lipin1^{Myf5cKO} mice were differentiated for 6 days and then treated with Fluo-4 for 30 minutes. After extensive washing with HBSS, Fluo-4 fluorescence images were acquired. Acquisition parameters were the same for all images obtained. Scale bars = 50 µm.

Table 1.

Muscle Force Data.

The average values for the muscle mass, frequency at which half the maximum force was generated ($f_{1/2}$), the peak absolute (N) and specific force (N/g) generated in response to a single stimulation (twitch), and the absolute (N) and specific force (N/g) generated in response to 100 Hz stimulation. Values shown as mean ± SD.

	Muscle Mass (mg)	$f_{1/2}$ (Hz)	Twitch (N)	Twitch (N/g)	100Hz (N)	100Hz (N/g)
Lipin1$^{fl/fl}$	205 ± 31.0	40.7 ± 6.6	1.11 ± 0.15	5.44 ± 0.56	3.73 ± 0.35	18.5 ± 2.87
Lipin1^{Myf5cKO}	133 ± 24.7	31.5 ± 6.2	0.66 ± 0.25	4.32 ± 1.13	2.35 ± 0.55	15.8 ± 1.39
mdx	263 ± 29.1	34.2 ± 12.3	0.86 ± 0.11	3.41 ± 0.48	2.32 ± 0.42	9.1 ± 1.29
DKO	158 ± 28.2	34.5 ± 5.1	0.59 ± 0.18	3.68 ± 0.66	1.62 ± 0.51	10.1 ± 2.12

Table 2.

Statistical Comparisons of Muscle Force Data.

A comparison of the mean values from Table 1. the p-values were determined from a one-way ANOVA with a post hoc Bonferroni comparison.

p-values						
Comparison	**Muscle Mass**	**$f_{1/2}$**	**Abs Twitch**	**Sp Twitch**	**Abs 100Hz**	**Sp 100Hz**
$Lipin1^{fl/fl}$ vs $Lipin1^{Myf5cKO}$	1.56513E-4	0.12586	5.21356E-5	0.01857	2.65564E-6	0.10345
$Lipin1^{fl/fl}$ vs mdx	0.00131	0.77504	0.08344	8.75483E-5	1.22214E-5	1.17017E-7
$Lipin1^{fl/fl}$ vs DKO	0.01638	0.7451	1.60871E-5	2.72649E-4	2.11488E-9	3.03855E-7
$Lipin1^{Myf5cKO}$ vs mdx	5.73055E-8	0.999	0.32473	0.24991	0.999	1.73192E-4
$Lipin1^{Myf5cKO}$ vs DKO	0.89443	0.999	0.999	0.77412	0.04007	7.44355E-4
mdx vs DKO	2.95024E-6	0.999	0.10503	0.999	0.09326	0.999